Chapter 3

Squeeze-Film Bearing Made up of Porous and Circumferentially Rough Discs with Micromodel Patterns of Porous Structures

Contents

3.1 Introduction

Ferrofluids (FFs) or magnetic fluids (MFs) [1] are stable colloidal suspensions containing fine ferromagnetic particles dispersing in a liquid, called carrier liquid, in which a surfactant is added to generate a coating layer preventing the flocculation of the particles. When an external magnetic field **H** is applied, FFs experiences magnetic body force $(\mathbf{M} \bullet \nabla)\ \mathbf{H}$ which depends upon the magnetization vector **M** of ferromagnetic particles. Owing to these features FFs are useful in many applications including bearing design systems related to squeeze-films [1-6]. Squeeze-film phenomenon arise because of two lubricated surfaces approach each other with a normal velocity. This normal velocity is called squeeze velocity. In many applications squeeze-film behaviour are observed like in bearings, machine tools, gears, rolling elements, hydraulic systems, engines, clutch plates, human knee joints, etc.

It is well known that bearing surfaces in practice are all rough and roughness is inherent in the manufacture of bearings, therefore, any realistic analysis of these bearings must consider the contacting surfaces as rough. Christensen [7] developed stochastic models for the study of hydrodynamic lubrication of rough surfaces in which one-dimensional circumferential and radial roughness patterns were discussed. Christensen *et. al.* [8] derived generalized form of Reynolds equation applicable to rough bearings by assuming the fluxes to be represented by power series of a stochastic film-thickness function. Depending on the Christensen's roughness model, Prakash and Tiwari [9] studied roughness effect on the squeeze-film between rotating porous annular discs with arbitrary porous wall thickness. An exact solution, valid for arbitrary wall thickness is given for the film pressure and pressure in the bearing material. Recently,

Bujurke *et. al.* [10] studied roughness effect on squeeze-film behaviour in porous circular discs with couple-stress fluid. They have shown that the effect of couple-stress fluid and surface roughness is more pronounced as compared to classical one. Naduvinamani *et. al*. [11] studied roughness effect on squeeze-film between porous circular stepped plates using couple-stress fluid. It was shown that the effect of magnetic field increase the mean load-carrying capacity and lengthen the mean squeeze time. Basti [12] discussed effect of surface roughness on squeeze-film between curved annular plates using couple-stress fluid. It was shown that the circumferential roughness pattern on the curved annular plate results in more pressure buildup whereas performance of the squeeze-film suffers due to the radial roughness pattern for both concave and convex plates.

With the advent of FFs, many researchers have tried to find its applications as lubricant. Agrawal [13] studied effects of MF on a porous inclined slider bearing and found that the magnetization of the magnetic particles in the lubricant increases load capacity without affecting the friction on the moving slider. Verma [14] studied squeeze-film bearing with MF as lubricant using three porous layers attached to the lower plate and show that load-carrying capacity increases due to the effect of MF lubricant as compared to conventional viscous fluid as lubricant. Chi *et. al.* [15] discuss new type of FF lubricated journal bearing consisting of three pads. One of them is a deformable elastic pad. The theoretical analysis and experimental investigation shows that the performance of the bearing is much better than that of ordinary bearings. Moreover, the bearing operated without leakage and any feed system. Recently, Uhlmann *et. al.* [16] discuss about application of MFs in tribotechnical systems. The

rheological and tribological behaviour of MFs was investigated and compared with conventional lubricants between friction pairs under boundary conditions. Ahmad and Singh [17] studied about MF lubricated porous pivoted slider bearing with slip velocity. There it was discussed that the minimization of the slip parameter and permeability parameter increases the load-carrying capacity. Singh and Gupta [18] studied about curved slider bearing with FF as lubricant and shown that the effect of rotation and volume concentration of magnetic particles improves the stiffness and damping capacities of the bearings. Shah and co-authors [19-28] studied about FF lubricated various designed bearings like porous slider bearings of different shapes, long journal bearing, axially undefined journal bearing, squeeze-film bearings with the inclusion of effects of slip velocity at the porous boundary, anisotropic permeability of the porous matrix, etc. More recently, Shah and Kataria [29] theoretically discussed FF based squeeze-film characteristics between a sphere and a flat porous plate. It is concluded that loss in dimensionless load-carrying capacity due to the effect of porosity is almost zero because of using FF as lubricant for smaller values of thickness parameter of the porous layer and radial permeability parameter. Shah and Patel [30] studied squeeze-film characteristics between a rotating sphere and a radially rough plate and shown that better performance of the dimensionless load-carrying capacity can be obtained w.r.t. various parameters.

The purpose of the present Chapter is to develop a mathematical model of FF lubricated flat annular squeeze-film bearing which is formed when a porous upper disc (plate or surface) approaches a circumferentially rough impermeable lower disc considering radially variable magnetic field (VMF). The roughness effect is presented

on the basis of Christensen's stochastic theory for hydrodynamic lubrication of rough surfaces [7,8]. The VMF is important because of its advantage of generating maximum field at the required active contact zone. Moreover, the magnetic field considered is oblique and maximum at the middle of the lower disc. The modified Reynolds equation is derived and its exact solution is obtained in terms of Bessel function. This method of solving Reynolds equation is important because it violets the assumption of replacing pressure in the porous matrix by the average pressure w.r.t. bearing wall thickness and then the average pressure equal to the film pressure at any section [31]. Dimensionless load-carrying capacity is calculated and discussed from different viewpoints. The effects of width of the porous layer, permeability, surface roughness, etc. are studied. The effects of micromodel patterns of two different porous structures suggested by Kozeny-Carman and Irmay [5,27] are also discussed. This study of different porous structures is important because it has significant effect on the bearing characteristics [27]. Moreover, the porous structures are also important because of self-lubricating property of the bearing design systems.

3.2 Mathematical Formulation of the Problem

The physical configuration of the problem of squeeze-film bearing made up of two flat annular discs is shown in figure 3.1. Both the discs are having inner radius b and outer radius a. A porous layer (disc or region or surface or matrix or facing) of thickness l is attached to the upper impermeable disc (solid housing) while the lower impermeable disc is circumferentially rough. Initially the two discs are separated by a lubricating film of FF (known as film region) with thickness h, where

$$h = h_n(t) + h_s(r,\theta,\xi),$$

(3.1)

which is made up of two parts as follows :

(1) $h_n(t)$ denotes the nominal, smooth part of the film geometry with *t* as time, and

(2) $h_s(r,\theta,\xi)$ is the part due to the surface asperities measured from the nominal level and is regarded as a randomly varying quantity of zero mean with *r* as radial co-ordinate, θ as angular co-ordinate and ξ as the index parameter determining a definite roughness arrangement.

During engagement, an axial force is applied to the upper disc and it starts to approach the lower one with a normal velocity (squeeze velocity) $\dot{h} = dh/dt$, till the mechanical contact is made.

While deriving the Reynolds equation, it is assumed that the flow is laminar, the fluid is incompressible and possesses constant properties, the porous matrix is homogeneous and isotropic, all the inertia terms can be neglected, flow in the film and the porous region is axisymmetric, derivatives of velocities across the film predominate and velocities are continuous at the interface between porous region and film region.

On the basis of these assumptions, the equation governing the pressure distribution *p* in the film region considering cylindrical polar co-ordinates in *r* – direction is obtained as

$$\frac{\partial}{\partial r}\left(p - \frac{1}{2}\mu_0 \bar{\mu} H^2 \right) = \eta \frac{\partial^2 u}{\partial z^2},$$

(3.2)

where *H* is strength of the radially VMF.

Using continuity equation (2.26) in cylindrical polar co-ordinates and integrating it w.r.t. z over the film-thickness [0, h] yields

$$\frac{1}{r}\frac{\partial}{\partial r}\int_0^h ru\, dz + w\big|_{z=h} = 0,$$

(3.3)

where $w\big|_{z=0} = 0$ as lower disc is impermeable.

Integrating equation (3.2) twice w.r.t. z and using boundary conditions

$u = 0$ when $z = 0$ and $u = 0$ when $z = h$,

the expression for u can be obtained, which on substituting in equation (3.3) yields

$$\frac{1}{r}\frac{\partial}{\partial r}\left[rh^3\frac{\partial}{\partial r}\left(p-\frac{1}{2}\mu_0\bar{\mu}H^2\right)\right] = 12\eta\, w\big|_{z=h}.$$

(3.4)

Using velocity components in the porous region governed by Darcy's law, equation (3.4) can be written as

$$\frac{1}{r}\frac{\partial}{\partial r}\left[rh^3\frac{\partial}{\partial r}\left(p-\frac{1}{2}\mu_0\bar{\mu}H^2\right)\right] = 12\eta\frac{dh}{dt} - 12\varphi\left[\frac{\partial}{\partial z}\left(P-\frac{1}{2}\mu_0\bar{\mu}H^2\right)\right]_{z=h}$$

(3.5)

with P satisfying the equation

$$\frac{1}{r}\frac{\partial}{\partial r}\left[r\frac{\partial}{\partial r}\left(P-\frac{1}{2}\mu_0\bar{\mu}H^2\right)\right] + \frac{\partial^2}{\partial z^2}\left(P-\frac{1}{2}\mu_0\bar{\mu}H^2\right) = 0,$$

(3.6)

where φ is the permeability of the porous facing and P is the pressure in the porous region.

Choosing oblique radially VMF strength H^2 of **H** as [6]

$$H^2 = K(r-b)(a-r),$$

(3.7)

so that it is maximum at the middle of the lower disc and vanishing at $r = b, a$. Here, K is a constant to be chosen to suit the dimensions of both sides.

The reason for choosing this H^2 lies in the observation that uniform magnetic field does not have any effect on the present analysis as can be seen from equation (3.2). Moreover, it has an advantage of generating maximum field at the required active contact zone. Here, active contact zone is considered at the middle of the lower disc. For other active contact zones, different forms of magnetic field should be chosen.

Using equation (3.7), equations (3.5) and (3.6), respectively, becomes

$$\frac{1}{r}\frac{\partial}{\partial r}\left(r\, h^3 \frac{\partial p}{\partial r}\right) - \frac{1}{2}\left(\frac{a+b}{r} - 4\right)\mu_0 \bar{\mu}\, K h^3 = 12\eta \frac{dh}{dt} - 12\varphi\left(\frac{\partial P}{\partial z}\right)_{z=h},$$

(3.8)

$$\frac{1}{r}\frac{\partial}{\partial r}\left(r\frac{\partial P}{\partial r}\right) + \frac{\partial^2 P}{\partial z^2} = \frac{1}{2r}\mu_0 \bar{\mu} K(b+a) - 2\mu_0 \bar{\mu} K.$$

(3.9)

Taking expected values of both sides of equation (3.8) yields

$$\frac{1}{r}\frac{\partial}{\partial r}\left[r\, E\left(h^3 \frac{\partial p}{\partial r}\right)\right] - \frac{1}{2}\left(\frac{a+b}{r} - 4\right)\mu_0 \bar{\mu} K\; E(h^3) = 12\eta \frac{dE(h)}{dt} - 12\varphi\left(\frac{\partial P}{\partial z}\right)_{z=h},$$

(3.10)

where expectancy operator $E(\bullet)$ is defined by

$$E(\bullet) = \int_{-\infty}^{\infty} (\bullet)\, f(h_s)\, dh_s$$

(3.11)

and f is the probability density function of the stochastic film-thickness h_s. Such a probability density function approximated by Christensen in [7,8] as

$$\begin{aligned} f(h_s) &= \frac{35}{32c^7}(c^2 - h_s^2)^3 \quad ; \quad -c < h_s < c \\ &= 0 \qquad\qquad\qquad\quad ; \quad \text{elsewhere} \end{aligned} \tag{3.12}$$

where c is the maximum asperity deviation from nominal film height and the function terminates at $c = \pm 3\tau$ with τ being the standard deviation.

Equation (3.10) is dependent on the structure of the surface roughness. In the context of stochastic theory, one-dimensional circumferential roughness is one of the roughnesses of special theoretical interest [7] and thus it is considered here for study. For one-dimensional circumferential roughness, the surfaces have the form of long, narrow ridges and valleys running in θ - direction, the film-thickness given by equation (3.1), therefore, assumes the form

$$h = h_n(t) + h_s(r, \xi). \tag{3.13}$$

For this type of roughness pattern, equation (3.10) reduces to

$$\frac{1}{r}\frac{d}{dr}\left[r \frac{1}{E(h^{-3})} \frac{dE(p)}{dr} \right] - \frac{1}{2}\left(\frac{a+b}{r} - 4 \right) \mu_0 \bar{\mu} K \frac{1}{E(h^{-3})} = 12\eta \frac{dE(h)}{dt} - 12\varphi \left(\frac{\partial P}{\partial z} \right)_{z=h}, \tag{3.14}$$

which is the required modified Reynolds equation for the present study.

3.3 Solution of the Problem

For solving equation (3.9), the following suitable boundary conditions are considered.

Assuming that there is zero ambient pressure at both the ends a and b of the porous facing, therefore

$$P(a,z)=0 \tag{3.15}$$

and

$$P(b,z)=0. \tag{3.16}$$

Also, assuming that there is no flow through the impervious boundary at the top of the porous disc, therefore

$$\frac{\partial P}{\partial z}=0 \text{ at } z=h+l. \tag{3.17}$$

With the above boundary conditions, solution of homogeneous problem of equation (3.9) using method of separable variable becomes

$$P=\sum_{n=1}^{\infty} C_n \, \mathrm{e}^{\alpha_n z}[1+\mathrm{e}^{2\alpha_n(h+l-z)}]U_0(\alpha_n r), \tag{3.18}$$

where C_n are constant coefficients and

$$U_0(\alpha_n r)=Y_0(\alpha_n a)J_0(\alpha_n r)-J_0(\alpha_n a)Y_0(\alpha_n r) \tag{3.19}$$

in which J_0 is the Bessel function of first kind of order zero, Y_0 is the Bessel function of second kind of order zero.

The $\alpha_n = (4n-1)\pi/4a$ is the n^{th}-eigenvalue which satisfies

$$U_0(\alpha_n b) = 0. \tag{3.20}$$

The complete solution of equation (3.9), therefore becomes

$$P = \sum_{n=1}^{\infty} C_n \, e^{\alpha_n z}[1 + e^{2\alpha_n (h+l-z)}]U_0(\alpha_n r) + \frac{1}{2}\mu_0 \bar{\mu} H^2. \tag{3.21}$$

Using (3.11),

$$E(h) = h_n \tag{3.22}$$

and

$$E(h^{-3}) = \frac{35}{32c^7}\left[3(5h_n^2 - c^2)(c^2 - h_n^2)\ln\frac{h_n + c}{h_n - c} + 2ch_n(15h_n^2 - 13c^2)\right]. \tag{3.23}$$

Equation (3.14), using equations (3.21), (3.22) becomes

$$\frac{1}{r}\frac{d}{dr}\left[r\frac{dE(p)}{dr}\right] = 12\eta E(h^{-3})\frac{dh_n}{dt} - 12\varphi E(h^{-3})\sum_{n=1}^{\infty}\overline{C}_n\alpha_n(1 - e^{2\alpha_n l})U_0(\alpha_n r) + \frac{1}{2}\left(\frac{a+b}{r} - 4\right)\mu_0\bar{\mu}K, \tag{3.24}$$

where

$$\overline{C}_n = C_n \, e^{\alpha_n h_n} \tag{3.25}$$

are constants to be determined.

Integrating equation (3.24) twice w.r.t. r and making use of the boundary conditions

$$E[p(a)] = 0,$$

(3.26)

$$E[p(b)] = 0,$$

(3.27)

which indicates zero ambient pressure at both the ends a and b of the film region, yields the mean pressure in the film region as

$$E(p) = 3\eta E(h^{-3})R(r)\frac{dh_n}{dt} + 12\varphi E(h^{-3})\sum_{n=1}^{\infty}\frac{\overline{C}_n}{\alpha_n}(1-e^{2\alpha_n l})U_0(\alpha_n r) + (r-b)(a-r)\frac{\mu_0\bar{\mu}K}{2},$$

(3.28)

where

$$R(r) = r^2 + \frac{(b^2-a^2)\ln r + a^2\ln b - b^2\ln a}{\ln a - \ln b}.$$

(3.29)

Considering the pressure continuity at the film-disc interface; that is

$$E[p(r)] = E[P(r,h)],$$

(3.30)

using equation (3.21) and orthogonality of eigenfunctions $U_0(\alpha_n r)$, yields

$$\overline{C}_n = -\frac{12\pi\eta E(h^{-3})\,\dot{h}_n\,J_0(\alpha_n b)}{\alpha_n[J_0(\alpha_n a) + J_0(\alpha_n b)]} \times \frac{1}{\left[(1+e^{2\alpha_n l})\alpha_n + 12\varphi(1+e^{2\alpha_n l})E(h^{-3})\tanh(\alpha_n l)\right]}.$$

(3.31)

Substituting this $\overline{C}_n$ in equation (3.28) implies

$$E(p) = -12\pi\eta E(h^{-3})\frac{dh_n}{dt} \times \sum_{n=1}^{\infty} \frac{J_0(\alpha_n b)U_0(\alpha_n r)}{\alpha_n[J_0(\alpha_n a) + J_0(\alpha_n b)]} \times \frac{1}{\alpha_n + 12\varphi E(h^{-3})\tanh(\alpha_n l)} + (r-b)(a-r)\frac{\mu_0\bar{\mu}K}{2}.$$

(3.32)

The definition of mean load-carrying capacity

$$E(W) = 2\pi\int_b^a E(p)rdr$$

(3.33)

implies

$$E(W) = -3\eta E(h^{-3})\frac{dh_n}{dt}\sum_{n=1}^{\infty}\left[\frac{16\pi\{J_0(\alpha_n b) - J_0(\alpha_n a)\}}{\alpha_n^3\{J_0(\alpha_n a) + J_0(\alpha_n b)\}} \times \frac{1}{\alpha_n + 12\varphi E(h^{-3})\tanh(\alpha_n l)}\right] + \frac{1}{12}\mu_0\bar{\mu}\pi K(a-b)^3(a+b)$$

(3.34)

with equation (3.23).

Here, permeability φ may be chosen in different way as follows.

$$\varphi = \begin{cases} \varphi & \text{, for arbitrary porous structures} \\ \dfrac{D_c^2\,\varepsilon^3}{180(1-\varepsilon)^2} & \text{, for globular spheres porous structures} \\ \dfrac{\left(1-m^{\frac{2}{3}}\right)\left(1-m^{\frac{1}{3}}\right)^2 D_s^2}{12m};\ m = 1-\varepsilon = \dfrac{D_s^3}{(D_s+b_1)^3} & \text{, for capillary fissures porous structures} \end{cases}$$

(3.35)

Defining dimensionless quantities

$$\Phi = \frac{\varphi}{h_n^2},\ \bar{l} = \frac{l}{h_n},\ \psi = \Phi\bar{l},\quad C = \frac{c}{h_n},\ \ k = \frac{a}{b},\ \bar{\alpha}_n = \alpha_n b,\ \ L = \frac{l}{b},\quad \mu^* = -\frac{K\mu_0\bar{\mu}h_n^3}{\eta\dot{h}_n},$$

(3.36)

the dimensionless load-carrying capacity can be obtained as

$$\bar{W} = -\frac{E(W)h_n^3}{\eta b^4\dot{h}_n} = 48\pi\sum_{n=1}^{\infty} J_0^*(\bar{\alpha}_n)\left\{G(C) + \frac{12\psi}{\bar{\alpha}_n L}\tanh(\bar{\alpha}_n L)\right\}^{-1} + \frac{1}{12}\mu^*\pi(k-1)^3(k+1),$$

(3.37)

where

$$J_0^*(\bar{\alpha}_n) = \frac{[J_0(\bar{\alpha}_n) - J_0(\bar{\alpha}_n k)]}{\bar{\alpha}_n^4\,[J_0(\bar{\alpha}_n) + J_0(\bar{\alpha}_n k)]},$$

(3.38)

$$G(C) = \left[\frac{35}{32C^7}\left\{3(5-C^2)(C^2-1)\ln\frac{1+C}{1-C} + 2C(15-13C^2)\right\}\right]^{-1}.$$

(3.39)

3.4 Results and Discussion

When FF is used as lubricant, then the variation in dimensionless load-carrying capacity $\bar{W}$ is due to the second term of the equation (3.37). The radially VMF considered is oblique to the lower disc and its strength is maximum at the middle of the disc $r = (a + b)/2$. The order of magnetic field strength for different K is shown in figure 3.2 when a = 0.075 (m) and b = 0.05 (m). The dimensionless load-carrying capacity is numerically calculated from different viewpoints and presented graphically for the representative values of different parameters given in section 3.4.3.

3.4.1 Discussion on Dimensionless Load-Carrying Capacity

Figure 3.3 shows the comparative study of variation in $\overline{W}$ as a function of dimensionless thickness of the porous matrix L for dimensionless permeability parameter for arbitrary porous structure $\Phi = 0.01390$ and $\Phi = 0.1390$. It is observed that $\overline{W}$ increases as L decreases. The increase rate of $\overline{W}$ is more for $\Phi = 0.1390$ when $L < 0.02$. In the same way the increase rate of $\overline{W}$ is more for $\Phi = 0.01390$ when $L < 0.2$. Moreover, the increase rate of $\overline{W}$ is more in the case of $\Phi = 0.01390$ as compared to $\Phi = 0.1390$.The maximum increase rate difference is observed when $L = 0.002$. At this L, $\overline{W} \approx 8$ for $\Phi = 0.1390$ and $\overline{W} \approx 21$ for $\Phi = 0.01390$, therefore, increase rate of $\overline{W}$ is almost 163 % more for $\Phi = 0.01390$ as compared to $\Phi = 0.1390$.

Figure 3.4 shows the variation in $\overline{W}$ as a function of dimensionless surface roughness parameter C for different values of L. It is observed that $\overline{W}$ increases as C increases for $0.0002 \leq L < 0.02$. After $L = 0.02$, the roughness effects become negligible. Also, for $C = 0.1179$ when $L = 0.2$, $\overline{W} \approx 1$ and when $L = 0.02$, $\overline{W} \approx 7$, therefore, the increase rate of $\overline{W}$ is almost 600% when $L = 0.02$. Similarly, for $C = 0.1179$ when $L = 0.002$, $\overline{W} \approx 16$, therefore the increase rate of $\overline{W}$ is almost 129% from $L = 0.02$ to $L = 0.002$.

From the above observations, the decreasing tendency of $\overline{W}$ w.r.t. increasing values of Φ and L may be interpreted by the physical process as under: According to [32], the pressure in the porous medium provides a path for the fluid to come out easily from the bearing to the environment. The higher the permeability, the more readily does

fluid flow through the porous material. In this way, the presence of the porous material decreases the resistance to flow in r – direction and as a consequence the load-carrying capacity is reduced. This behaviour of decreasing load-carrying capacity with the insertion of porous matrix and higher permeability also agrees with the conclusions of Prakash and Tiwari [33] while discussing the problem of squeeze-film of rough porous rectangular plates theoretically and experimentally by Wu [34]. In our case, the above behaviour of $\overline{W}$ w.r.t. Φ and L matches because it may be possible that in the porous matrix the FF effect may be less and the FF behaves like conventional fluid under the action of magnetic field. Moreover, it is observed that the increasing effect of surface roughness increases the load-carrying capacity. This may be because of the generation of spikes due to presence of FF in the surface pattern and retention of the fluid therein (which resist the mechanical contact of the upper and lower surfaces).

Figure 3.5 shows the variation in $\overline{W}$ as a function of dimensionless parameter k, which is ratio of outer radius a by inner radius b defined in equation (3.36), for different values of L. It is observed that $\overline{W}$ increases as k increases; that is, as the width of the annular part $b \le r \le a$ increases. This is because FF in the presence of magnetic field generates spikes and greater the generation of spikes may lead to better load-carrying capacity because of their strength. In addition, it can be seen from Table 3.1 that just by smaller increasing change in the value of k; that is, increasing width of the annular part, the rate of $\overline{W}$ increases suddenly and jumps to higher value. Thus, the smaller change in k results greater change in $\overline{W}$.

3.4.2 Effects of Two Different Micromodel Patterns of Porous Structures

When the porous matrix designed with micromodel pattern of globular spheres suggested by Kozeny-Carman [5,27], then the permeability of the upper porous matrix as defined in equation (3.35) is given by

$$\varphi = \varphi_g = \frac{D_c^2\ \varepsilon^3}{180(1-\varepsilon)^2},$$

where D_c is a mean particle size and ε is the porosity of the porous matrix (Refer Figure 3.6).

Similarly, when the porous matrix designed with micromodel pattern of capillary fissures composed of three sets of mutually orthogonal fissures as suggested by Irmay [5,27], then the permeability of the upper porous matrix as defined in equation (3.35) is given by

$$\varphi = \varphi_f = \frac{\left(1-m^{\frac{2}{3}}\right)\left(1-m^{\frac{1}{3}}\right)^2 D_s^2}{12m};\ m = 1-\varepsilon = \frac{D_s^3}{(D_s+b_1)^3},$$

where D_s is a mean solid size and b_1 is the thickness of the fissure (Refer Figure 3.7).

By considering sample values

$$\varepsilon = 0.2,\ D_c = D_s = 0.000007\,(\mathrm{m}),$$

the value of the dimensionless permeability parameter Φ for the both the cases can be obtained respectively as follows.

$$\Phi_g = \frac{\varphi_g}{h_n^2} = 4.7297\times10^{-7}\ \text{(For globular sphere model)}$$

$$\Phi_f = \frac{\varphi_f}{h_n^2} = 5.0390 \times 10^{-7} \text{ (For capillary fissures model)}$$

From the above value of Φ, it is observed that $\Phi_g < \Phi_f$; that is, for the same data values, the permeability obtained in the case of globular sphere model is less. From figure 3.8, it is observed that up to $L = 0.02$, $\overline{W}$ almost remains same and constant for both the porous structures. But after that $\overline{W}$ decreases. It is also observed that there is a moderate difference in the decrease rate between both the porous structures. The slightly better performance of $\overline{W}$ is obtained in the case of globular structure.

Limiting Cases

(1) When $H^2 \to 0$, the present analysis reduces to [9] for nonmagnetic case without rotation effect.

(2) When $H^2 \to 0$, $\varphi \to 0$ or $l \to 0$, the present case reduces to [31], which is approximated under the assumption that the pressure in the film at any section is equal to the average pressure in the bearing matrix at that section.

(3) When $H^2 \to 0$, $C \to 0$, the present case reduces to smooth porous surfaces [35] without rotation effect.

(4) When $C \to 0$, the present case reduces to [6] for exponential pad of the upper surface.

3.4.3 Representative Values and Formula for Bessel Function

The following representative values are taken in computations which are common for all figures and table.

$$h_n = 8.482 \times 10^{-5}\,(\text{m}), \eta = 0.012\,(\text{Nsm}^{-2}), \bar{\mu} = 0.05,$$
$$\mu_0 = 4\pi \times 10^{-7}\,(\text{NA}^{-2}), \dot{h}_n = -0.08\,(\text{ms}^{-1})$$

Values taken for different figures are as follows:

For figure 3.3: $a = 0.075$ (m), $b = 0.05$ (m), $c = 0.000030$ (m), $\varphi = 10^{-9}$ (m^2),

$\varphi = 10^{-10}$ (m^2), $K = 10^{10}/1.56(A^2/m^4)$ so that $O(H) \approx 3$.

For figure 3.4: $a = 0.075$ (m), $b = 0.05$ (m), $\varphi = 10^{-10}$ (m^2), $c = 0.00001$ (m),

$c = 0.000015$ (m), $c = 0.000020$ (m), $c = 0.000025$ (m),

$c = 0.000030$ (m), $K = 10^{10}/1.56(A^2m^{-4})$ so that $O(H) \approx 3$.

For figure 3.5: $a = 0.075$ (m), $\varphi = 10^{-10}$ (m^2), $c = 0.000030$ (m),

($b = 0.02$ (m), $K = 10^{10}/7.5625(A^2m^{-4})$),

($b = 0.03$ (m), $K = 10^{10}/5.0625$ (A^2m^{-4})),

($b = 0.04$ (m), $K = 10^{10}/3.0625$ (A^2m^{-4})) ,

($b = 0.05$ (m), $K = 10^{10}/1.56$ (A^2m^{-4})) so that $O(H) \approx 3$.

For figure 3.8: $a = 0.075$ (m), $b = 0.05$ (m), $c = 0.000030$ (m),

$K = 10^{10}/1.56$ (A^2m^{-4}) so that $O(H) \approx 3$.

Here, $O(H)$ indicates the order of magnetic field strength.

Also, the formula for Bessel function of order zero considered in the calculation is [36]

$$J_0(x) = \left(\frac{1}{6}\right) + \left(\frac{1}{3}\right)\cos\left(\frac{x}{2}\right) + \left(\frac{1}{3}\right)\cos\left(\frac{\sqrt{3}x}{2}\right) + \left(\frac{1}{6}\right)\cos x,$$

and in equation (3.37), the summation extends for 10000 terms.

3.5 Conclusions

Based on the ferrohydrodynamic theory by R.E. Rosensweig and stochastic theory for hydrodynamic lubrication by Christensen, the present Chapter developed a mathematical model of FF lubricated flat (parallel) discs squeeze-film bearing which formed when a porous annular upper disc approaches a circumferentially rough

impermeable annular lower disc considering radially VMF. The VMF is important because of its advantage of generating maximum field at the required active contact zone. The magnetic field used is oblique and maximum at the middle of the lower disc. Moreover, porosity is considered because of getting advantageous property of self-lubrication. The modified Reynolds equation is derived and its exact solution is obtained in terms of Bessel function. This method of solving Reynolds equation is important because it violets the assumption of replacing pressure in the porous matrix by the average pressure w.r.t. bearing wall thickness and then the average pressure equal to the film pressure at any section [31]. Dimensionless load-carrying capacity is calculated and discussed for the effects of width of the porous layer, permeability, surface roughness, etc. The effects of micromodel patterns of two different porous structures defined by globular sphere model and capillary fissures model are also discussed. The following conclusions can be drawn from results and discussion.

$\overline{W}$ increases when

(1) thickness of porous matrix attached to the above disc decreases

(2) permeability of the porous matrix decreases

(3) effect of surface roughness increases

(4) width of the annular part increases

Moreover, slightly better performances of the bearing are observed in the case of globular sphere permeability model suggested by Kozeny-Carman. The VMF is having a significant effect on the problem as uniform magnetic field does not have any effect as can be seen from equation (3.2). It is believed that the predictions obtained from the results are useful for the bearing design Engineers.

3.6 Table

	K			
	1.5	1.875	2.5	3.75
$\overline{W}$	24.7386	62.2777	197.7555	986.6270
% variation in $\overline{W}$ as compared to k =1.5	0	151.7(↑)	699.4(↑)	3888.2(↑)

Table 3.1

Effect on $\overline{W}$ for different values of k when L = 0.0002

3.7 Figures

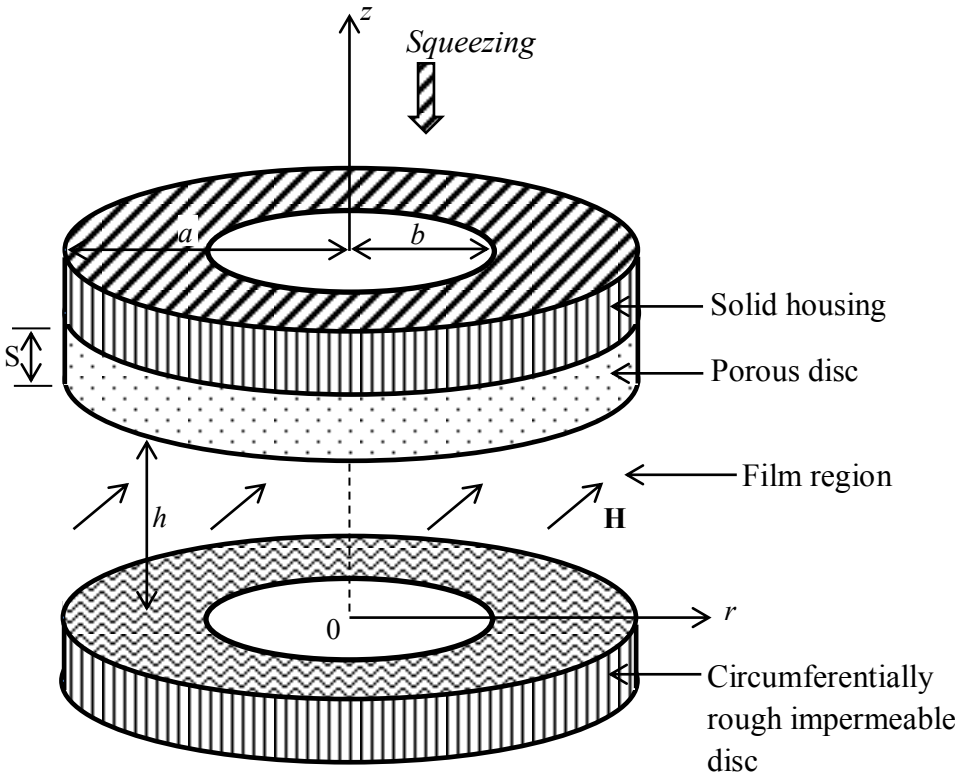

Figure 3.1

Schematic diagram of the squeeze-film bearing configuration between porous and circumferential rough discs

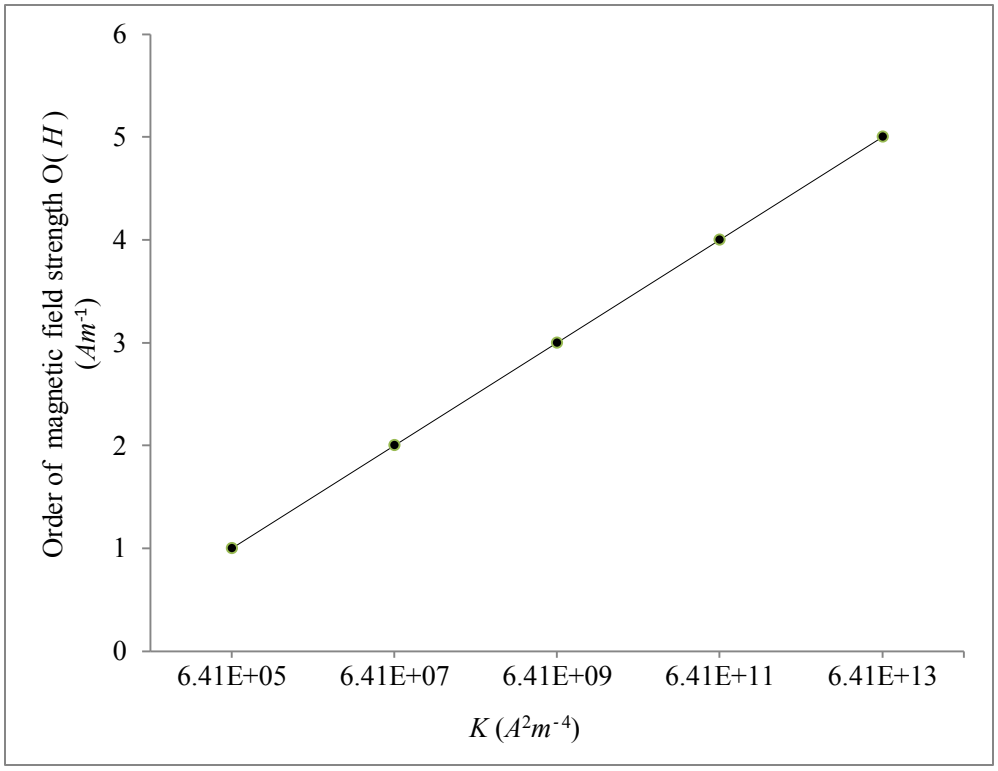

Figure 3.2

Order of magnetic field strength for different values of K when $k = 1.5$

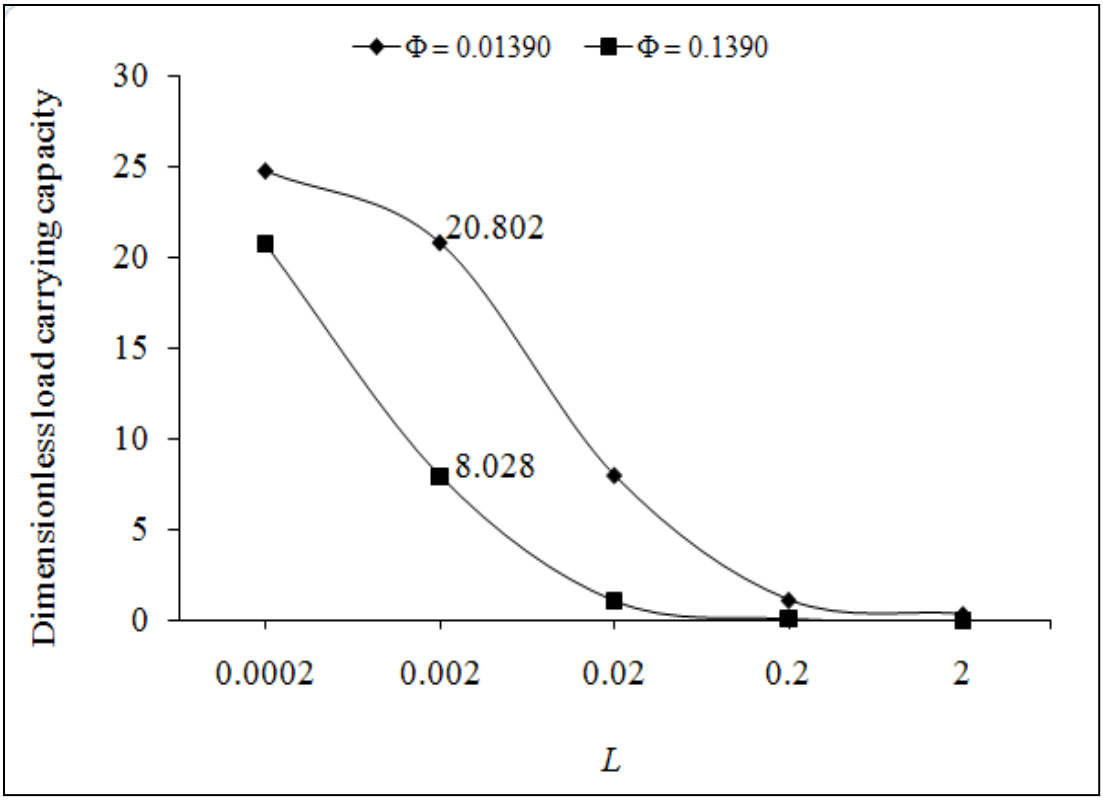

Figure 3.3

Variation in dimensionless load-carrying capacity $\overline{W}$ for different values of dimensionless thickness of the porous matrix L and dimensionless permeability parameter for arbitrary porous structure Φ

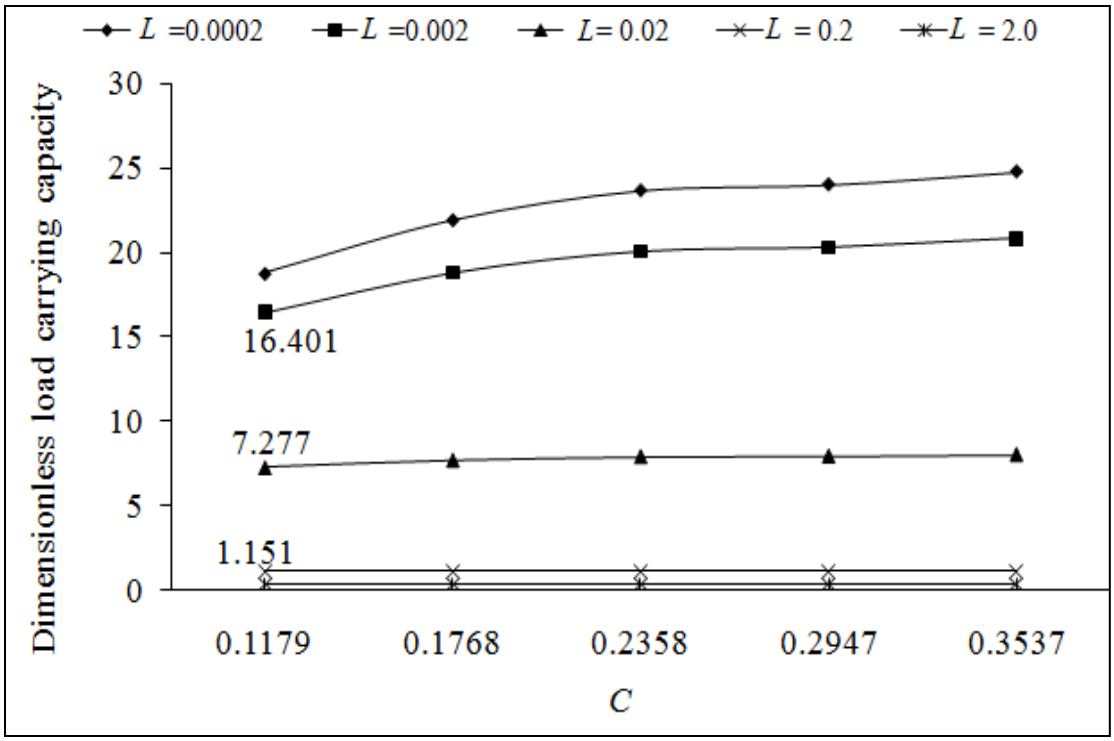

Figure 3.4

Variation in dimensionless load-carrying capacity $\overline{W}$ for different values of dimensionless roughness parameter C and dimensionless thickness of the porous matrix L

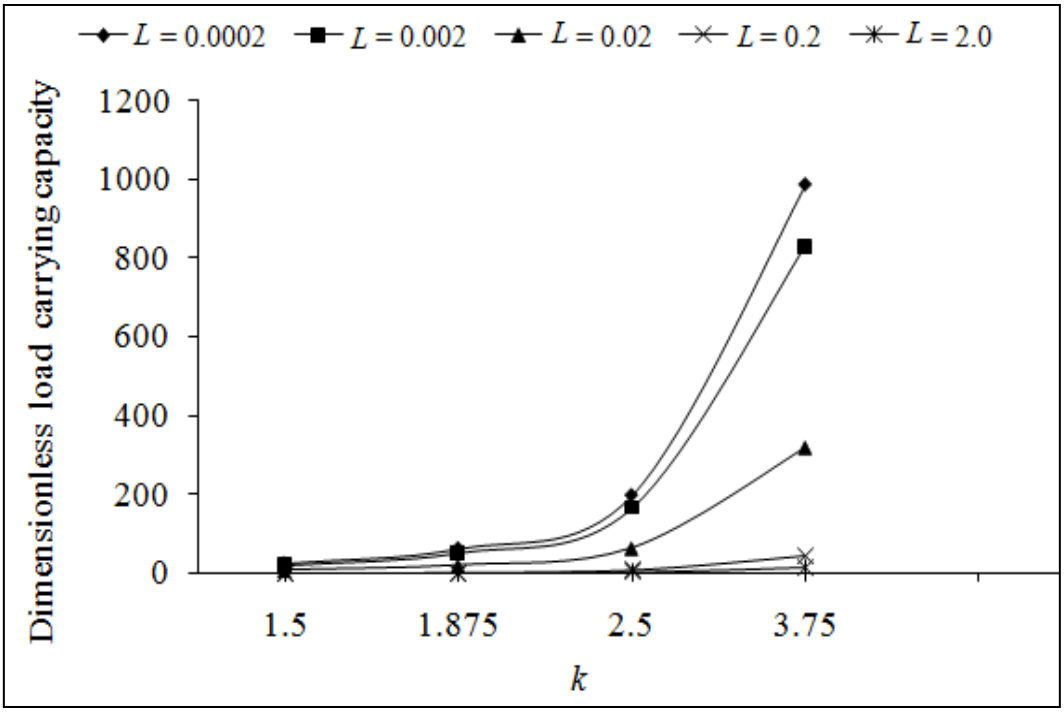

Figure 3.5

Variation in dimensionless load-carrying capacity $\overline{W}$ for different values of k and dimensionless thickness of the porous matrix L

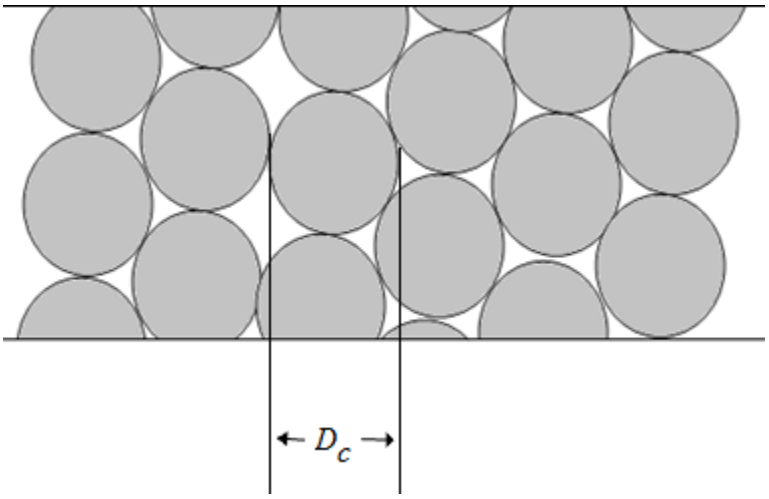

Figure 3.6

Micromodel globular sphere model of porous matrix suggested by Kozeny-Carman

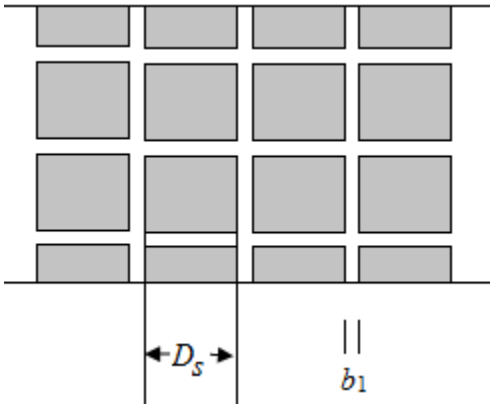

Figure 3.7

Micromodel capillary fissures model of porous matrix suggested by Irmay

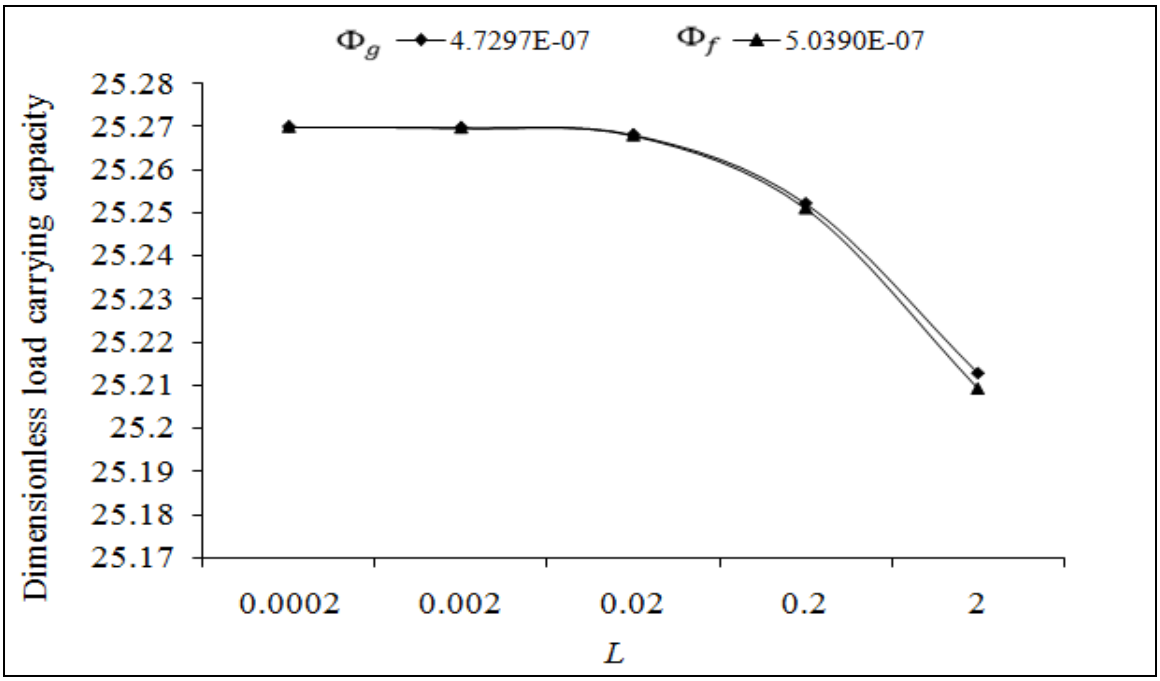

Figure 3.8

Variation in dimensionless load-carrying capacity $\overline{W}$ for different values of dimensionless roughness parameter C and dimensionless thickness of the porous matrix L and dimensionless permeability parameter in globular and capillary fissures model

3.8 References

1. R.E. Rosensweig, Ferrohydrodynamics, *Cambridge University Press*, New York, 1985.
2. V.G. Bashtovoi and B.M. Berkovskii, Thermomechanics of ferromagnetic fluids, *Magnitnaya Gidrodinamika* 3 (1973) 3-14.
3. N.C. Popa, I. Potencz, L. Brostean and L. Vekas, Some applications of inductive transducers with magnetic fluids, *Sensors and Actuators A* 59 (1997) 197-200.
4. R.V. Mehta and R.V. Upadhyay, Science and technology of ferrofluids, *Current Science* 76 (3) (1999) 305-312.
5. J. Liu, Analysis of a porous elastic sheet damper with a magnetic fluid, *Journal of Tribology* 131 (2009) 0218011-15.
6. R.C. Shah, S.R. Tripathi and M.V. Bhat, Magnetic fluid based squeeze-film between porous annular curved plates with the effect of rotational inertia, *Pramana-Journal of Physics* 58(3) (2002) 545-550.
7. H. Christensen, Stochastic models for hydrodynamic lubrication of rough surfaces, *Proc. Inst. Mech. Eng. (Part J)* 184 (55) (1969) 1013-1026.
8. H. Christensen, J.B. Shukla and S. Kumar, Generalized Reynolds equation for stochastic lubrication and its application, *Journal of Mechanical Engineering Science* 17 (1975) 262-270.
9. J. Prakash and K. Tiwari, Effect of surface roughness on the squeeze-film between rotating porous annular discs with arbitrary porous wall thickness, *International Journal of Mechanical Science* 27(3) (1985) 135-144.

10. N.M. Bujurke, D.P. Basti and R. B. Kudenatti, Surface roughness effects on squeeze-film behaviour in porous circular disks with couple stress fluid, *Transp. Porous Med*. 71 (2008) 185-197.

11. N. B. Naduvinamani, B. N. Hanumagowda and S.T. Fathima, Combined effects of MHD and surface roughness on couple-stress squeeze-film lubrication between porous circular stepped plates, *Tribology International* 56 (2012) 19–29.

12. D.P. Basti, Effect of surface roughness and couple stresses on squeeze-films between curved annular plates, *ISRN Tribology*, Volume 2013, Article ID 640178, 8 pages.

13. V.K. Agrawal, Magnetic fluid based porous inclined slider bearing, *Wear* 107 (1986) 133-139.

14. P. D. S. Verma, Magnetic fluid – based squeeze-film, *International Journal of Engineering Science* 24(3) (1986) 395-401.

15. C.Q. Chi, Z.S. Wang and P.Z. Zhao, Research on a new type of ferrofluid – lubricated journal bearing, *Journal of Magnetism and Magnetic Materials* 85 (1990) 257-260.

16. E. Uhlmann, G. Spur, N. Bayat and R. Patzwald, Application of magnetic fluids in tribotechnical systems, *Journal of Magnetism and Magnetic Materials* 252 (2002) 336–340.

17. N. Ahmad and J. P. Singh, Magnetic fluid lubrication of porous-pivoted slider bearing with slip velocity, *Journal of Engineering Tribology* 221 (2007) 609-613.

18. U. P. Singh and R. S. Gupta, Dynamic performance characteristics of a curved slider bearing operating with ferrofluids, *Advances in Tribology, Article ID* 278723 (2012) 6 pages.

19. R. C. Shah and M. V. Bhat, Ferrofluid lubrication in porous inclined slider bearing with velocity slip, *International Journal of Mechanical Sciences* 44 (2002) 2495-2502.

20. R. C. Shah and M. V. Bhat, Effect of slip velocity in a porous secant-shaped slider bearing with a ferrofluid lubricant, *FIZIKA A* 12 (1) (2003) 1-8.

21. R. C. Shah and M. V. Bhat, Ferrofluid lubrication equation for porous bearings considering anisotropic permeability and slip velocity, *Indian Journal of Engineering & Materials Sciences* 10 (2003) 277-281.

22. R. C. Shah and M. V. Bhat, Ferrofluid squeeze-film in a long journal bearing, *Tribology International* 37 (2004) 441- 446.

23. R. C. Shah and M. V. Bhat, Ferrofluid lubrication of a porous slider bearing with a convex pad surface considering slip velocity, *International Journal of Applied Electromagnetics and Mechanics* 20 (2004) 1-9.

24. R. C. Shah and M. V. Bhat, Anisotropic permeable porous facing and slip velocity on squeeze-film in an axially undefined journal bearing with ferrofluid lubricant, *Journal of Magnetism and Magnetic Materials* 279 (2004) 224-230.

25. R. C. Shah and M. V. Bhat, Magnetic fluid lubrication of bearing, each having a porous faced stator and a slider having various shapes, *Magnetohydrodynamics* 40(1) (2004) 91-97.

26. R. C. Shah, Effect of rotation on ferrofluid based squeeze-film of various shapes between two annular plates, *International Journal of Applied Mechanics and Engineering* 12(2) (2007) 515-525.

27. R. C. Shah and D. B. Patel, Squeeze-film based on ferrofluid in curved porous circular plates with various porous structure, *Applied Mathematics* 2 (2012) 121-123.

28. R. C. Shah and D. B. Patel, Mathematical analysis of newly designed ferrofluid lubricated double porous layered axially undefined journal bearing with anisotropic permeability, slip velocity and squeeze velocity, I*nternational Journal of Fluid Mechanics Research* 40 (5) (2013) 446-454.

29. R. C. Shah and R. C. Kataria. On the squeeze-film characteristics between a sphere and a flat porous plate using ferrofluid. *Applied Mathematical Modelling* 40 (2016) 2473-2484.

30. R. C. Shah and D. A. Patel, On the ferrofluid lubricated squeeze-film characteristics between a rotating sphere and a radially rough plate, *Meccanica*. DOI: 10.1007/s11012-015-0337-3.

31. J. Prakash and K. Tiwari, Effect of surface roughness on the squeeze-film between rotating porous annular discs, *Journal of Mechanical Engineering Science* 24 (1982) 155-161

32. E. M. Sparrow, G. S. Beavers and I. T. Hwang, Effect of velocity slip on porous walled squeeze-films, *Journal of Lubrication Technology* 94 (1972) 260-265.

33. J. Prakash and K.Tiwari, Lubrication of a porous bearing with surface corrugations, *Journal of Lubrication Technology* 104 (1982) 127-134.

34. H. Wu, A review of porous squeeze-films, *Wear* 47(1978) 371-385.

35. H. Wu, The squeeze-film between rotating porous annular disks, *Wear* 18 (1971) 461-470.

36. M. T. Abuelma'Atti, Trigonometric approximations for some Bessel functions, *Active and Passive Elec. Comp*. 22 (1999) 75-85.